MIJST
MIST International Journal of Science and Technology

Neutronic Analysis of BEAVRS PWR at Hot Zero Power Condition and Validation of SuperMC for PWR Assembly using OpenMC

Syeda Umme Kulsum Sadia*, Mohammad Taha Khan and Abdus Sattar Mollah

Department of Nuclear Science Engineering, Military Institute of Science and Technology, Dhaka, Bangladesh

***Corresponding Email:** *ummekulsum2421@gmail.com*

ARTICLE INFO

Article History:

Received: 10th September 2025
Revised: 06th March 2026
Accepted: 23rd May 2026
Published: 30th June 2026

Keywords:

Pressurized Water Reactor
Monte Carlo Simulation
SuperMC
OpenMC
BEAVRS

ABSTRACT

This paper contains various neutronic analyses on a pressurized water reactor (PWR). The model used in this work is the Benchmark for Evaluation and Validation of Reactor Simulations (BEAVRS) PWR with a thermal power of 3411 MW. The BEAVRS benchmark gives precise information about the two cycles of the 4-loop Westinghouse PWR core for Hot Full Power (HFP) and Hot Zero Power (HZP) conditions. The open-source Monte Carlo particle transport code OpenMC and the demo version of SuperMC have been used to determine the neutronic parameters and generate the respective graphs. ENDF/B-VIII.0, and JEFF-3.3 nuclear cross-section data libraries were used in OpenMC to calculate various core neutronic parameters for a continuous energy source, which includes the effective multiplication factor, changes in reactor parameters for various temperatures and enrichments of fuel element, Shannon entropy, fuel assembly burnup calculations, flux per lethargy, pin-by-pin thermal neutron flux distribution, and fission rate distribution across the core. The effective multiplication factor for different nuclear cross-section libraries was compared to visualize differences. Changes in criticality due to various geometric modifications, such as the core barrel, neutron shield panels, control rods, and burnable absorbers, have been observed using OpenMC, with a standard deviation of +/-0.00008 to +/-0.00009. The study provides a high-resolution, pin-by-pin, normalized thermal-neutron flux distribution, revealing a precise visualization of power peaking and flux gradients across varying fuel enrichment zones. This paper also aims to validate the burnup of a pre-built 7x7 PWR-alike assembly in the SuperMC interface and reconstruct it in OpenMC to compare the results. For the source type, a point source was selected at the centre of the assembly to run the simulation. The results show a resemblance to the descending trend of criticality with increasing burnup steps. The OpenMC and SuperMC methods implemented for PWR-based BEAVRS benchmark problems can also be applied to the PWR-type VVER-1200 reactor at the Rooppur Nuclear Power Plant, which is expected to become operational around 2026–2027.

1. INTRODUCTION

BEAVRS 3.0.2 is an updated version of the previously introduced Benchmark for Evaluation and Validation of Reactor Simulations (BEAVRS) by the MIT Computational Reactor Physics Group (Horelik et al., 2013). It provides detailed specifications of a commercial Westinghouse four-loop Pressurized Water Reactor, including material compositions, pin-resolved core geometry, and operational data for two cycles of operation (Hot Zero Power and Hot Full Power). It is specifically designed to validate various advanced computational tools for neutron transport and multi-physics simulations. It has been widely adopted for the verification of high-fidelity neutronic and coupled neutronic-thermal-hydraulic codes due to its high geometric and material fidelity, including realistic enrichment configurations, burnable absorbers, soluble boron, and control rods. With continuous updates to this benchmark, various geometrical refinements to the PWR core model have been introduced, and the latest version includes the correct number of control rod banks. OpenMC is a Monte Carlo code for photon and neutron transport, capable of executing computations on models with constructive solid geometry or CAD representation. It has an adaptable tally system for enumerating and analyzing various physical quantities. OpenMC uses a hybrid MPI and OpenMP programming model and has undergone extensive testing on supercomputers. It has comprehensive programming interfaces in Python and C/C++, facilitating pre- and post-processing, depletion calculations, workflow automation, multigroup cross-section generation, multiphysics coupling, and visualization of geometry and tally outcomes. It also features a Python-based nuclear data interface for advanced users to examine, modify, and execute tasks on HDF5, ACE, and ENDF files (Romano et al., 2015). SuperMC is an interactive Monte Carlo simulation platform designed by the FDS team to determine various neutronics parameters using the ENDF/B-7.1 nuclear cross-section data library (Wu et al., 2014). It is also capable of calculating radiation source terms/doses, transmutation, radiation shielding, and nuclear material depletion. CAD-based geometric modeling makes designing reactor cores or assemblies much easier.

Since the publication of the first BEAVRS benchmark, it has been used worldwide to validate various codes. Validation of the nodal diffusion code Serpent-ARES with the BEAVRS initial core at HZP condition was accomplished in 2014. The Finnish Radiation and Nuclear Safety Authority (STUK) and VTT Technical Research Centre of Finland collaborated to complete the study, which verified the Serpent-ARES code sequence for fuel-cycle simulation. It presented the first phase of the initial core, which involved HZP conditions. The results from the ARES nodal diffusion code were compared with those from a three-dimensional Serpent-generated code (Leppänen et al., 2014). Neutron transport calculations were performed using a diffusion model, such as TEDM, and a successful comparison between Serpent-calculated parameters and measured data (Pediz et al., 2023). The development of high-fidelity Multiphysics simulators, such as KANT, can effectively calculate neutronic core parameters while accounting for the complex distribution of fission (Oh et al., 2023). The BEAVRS benchmark was analyzed with nTRACER, a direct whole-core calculation code, in 2015. Control rod worth, depletion results from the first and reload cycles, the boron let-down curve, and detector signal comparisons with the nTRACER-calculated results confirmed the high accuracy of the error calculation for both cycles (Ryu et al., 2015).

Validation of the Serpent-ARES code continued for the Hot Full Power condition and fuel cycle 1 simulation. However, in this case, the calculated assembly power differed from the reference values because the assembly lattices were in an infinite condition (Leppänen et al., 2016). PWR large-scale burnup calculations have been simulated using RMC and coupled with the thermal-hydraulics sub-channel code COBRA (Liu et al., 2016), and later simulated multiple burnup cycles with continuous energy in a Hot Full Power condition (Wang et al., 2017). Another GPU-based continuous-energy Monte Carlo code, PRAGMA, specifically solved this PWR model for tests such as zero-power physics and depletion calculations (Kim et al., 2023). This model was validated with SuperMC at the HZP condition in 2017. Different neutronic parameters, including the effective multiplication factor, pin-by-pin power, control rod worth, temperature coefficient, and fission rate, were calculated using multiple Monte Carlo codes to verify the results; some of these showed good accuracy (Wang et al., 2017). Calculation from a single-fuel-pin cell to the whole core has been performed using the NECP-Bamboo code, which primarily performs fuel management (Li et al., 2018; Yang et al., 2021). SCALE 6.1.2 and PARCS 3.2, with the depletion sequence TRITON and the NEWT solver, were used for several calculations, including HZP measurements (Darnowski & Pawluczyk, 2019; Darnowski & Pawluczyk, 2022). Later, using updated versions of SCALE/Polaris 6.3.0 and PARCS 3.4.2, uncertainty analyses were conducted for various parameters (Kim et al., 2024).

An MCS-based coupled code system between CTF and FRAPCON was developed to first test a single-fuel-pin model and then a whole-core model to assess the thermal conductivity of the fuel and gap (Yu et al., 2019a). The same coupled code system performed depletion analyses of cycle 1 (Yu et al., 2019b) and cycle 2 (Yu, Lee, Kim, et al., 2019) to assess fuel performance. Back in 2020, using the neutronic code DeCART and a couple of MATRA codes, this model was verified with DeCART by calculating the control rod worth, the critical boron concentration, the radial detector signal, and the temperature coefficient. The differences in results from the neutronic code DeCART and the coupled code MATRA were not large, validating both codes for analyzing the BEAVRS model (Park et al., 2020). Besides this, DeCART/MIG was used for uncertainty quantification modeling, and it is widely accepted as a safety margin tool (Park & Cho, 2023). Validation of CASMO5/SIMULATE5 with nuclear data library ENDF/B-VII.1, ENDF/B-VIII.0 and JENDL-4.0 were used to perform several analyses along with a comparison between the measurement and benchmark data (Tatsuya et al., 2021; Bahadir, 2021). Later, differences between the calculated results of JENDL versions 4.0 and 5.0 were analyzed (Suzuki & Nagaya, 2023). Simulation of this model is also often done by using a core simulator called VERA (Virtual Environment for Reactor Applications), which provides direct solutions for neutronics, thermal-hydraulics, and coupled codes (Collins et al., 2020) (Albugami et al., 2023).

WIMS-ANL, a lattice code for cross-section generation, was validated using this benchmark. WIMS-ANL generated the first macroscopic cross-sections, and, using those cross-sections in the PARCS code, the axial power distribution across the assemblies was achieved (Coloma et al., 2022). In the same year, a sub-channel code, SUBCHANFLOW, was coupled with the nodal neutronics code Serpent-ANTS, and the coupled code was used to compare results from the depletion of a single fuel assembly in the BEAVRS first cycle (Valtavirta et al., 2022) and from pin-by-pin calculations (Tuominen & Valtavirta, 2022). Verification and validation of the pinwise nodal core calculation code, VANGARD, were performed in 2024 by analyzing this PWR model. For Hot Zero Power conditions, the control rod worth, critical boron concentration, and temperature coefficient depicted satisfactory results with high accuracy. In the Hot Full Power condition, the depletion results showed a small variation in the critical boron calculation

(Jeon et al., 2024). OpenMC and DDC-3D codes were validated by calculating various neutronic parameters and performing thermal-hydraulic analysis at both HZP and HFP in 3D whole-core simulations to assess accident-tolerant cladding materials (Alamri et al., 2024). The highest accuracy of the fission reaction rate in pincells of BEAVRS PWR, validated by deterministic simulation using OpenMOC, demonstrated the code's robustness and identified a cheaper neutronic analysis method that may reduce simulation time and boost efficiency in the future (Zhang et al., 2024; Gunow et al., 2019).

According to recent studies, artificial neural networks and Long Short-Term Memory (LSTM) can predict neutron transport and core neutronic parameters (Ren et al., 2023; Palmi et al., 2024). Analysis of fission distribution behavior in asymmetrical fuel assemblies with different homogenization and reflectors (Fröhlicher et al., 2021). Thermal neutron fluxes in different assemblies, calculated using MCNP6, showed good agreement with detector data (Hassan, 2020; Hassan & Hassan, 2021).

Though several works are validating the neutron flux across the core, none of them contain the neutron flux demonstration at every point of the core. This research aims to fill the data gap for BEAVRS PWR by providing a high-resolution, pin-by-pin normalized flux distribution map and a visualization of fission rates across every pincell of the core. Also, validation of the SuperMC demo version with limited resources has been completed.

2. MATERIALS AND METHODS

To start a neutronic analysis of a core, many parameters are needed to construct the geometry, assign materials, and calculate burnup. These parameters are often obtained from a literature review. For BEAVRS PWR, these parameters are included in Table 1-6 (Horelik et al., 2013).

2.1. BEAVRS Benchmark Specifications

Table 1: Core lattice parameters of BEAVRS PWR and loading pattern of fuel (Horelik et al., 2013)

Core Lattice	
Fuel assembly number	193
Loading pattern	w/o U-235
Region 1 (cycle no. 1)	1.60
Region 2 (cycle no. 1)	2.40
Region 3 (cycle no. 1)	3.10
Region 4A (cycle no. 2)	3.20
Region 4B (cycle no. 2)	3.40
Heavy metal loading for cycle no.1	81.8 MT

Table 2: Fuel assembly parameters of BEAVRS PWR (Horelik et al., 2013)

Fuel Assemblies	
Configuration of Pin lattice	17×17
Active length of fuel	365.76 cm
Fuel rod number	264
Spacer grid number	8

Table 3: Control parameters of BEAVRS PWR (Horelik et al., 2013)

Control parameters	
Material for the control rod (in the upper region)	B_4C
Material for the control rod (in the lower region)	Ag-In-Cd
Control rod bank number	57
Burnable poison rod number in the core	1266
Material for burnable poison	12.5 w/o B_2O_3

Table 4: Performance parameters of BEAVRS PWR (Horelik et al., 2013)

Performance	
Core (Thermal) power	3411 MW
Pressure during operation	2250 psia
Coolant flow rate through the core	61.5×10^6 kg/hr (5% bypass)

Table 5: Fuel assembly parameters of BEAVRS PWR (Horelik et al., 2013)

Property	Value
Pitch of assembly lattice	21.50364 cm
Pitch of pin lattice	1.25984 cm
Configuration of pin lattice	17 × 17
Fuel rod number	264
Guide tube number	24
Instrument tube number	1
Spacer grid number	8
Material for spacer grid (top/bottom)	Inconel 718

Material for grid sleeve (top/bottom)	Stainless Steel 304
Intermediate spacer grid and grid sleeve material	Zircaloy
Weight of Inconel (top/bottom grid)	390.136 g
Stainless Steel weight (top/bottom grid)	91.0329 g

Table 6: Structural component specifications of BEAVRS PWR (Horelik et al., 2013)

Property	Value
Width of baffle	2.22250 cm
Gap of baffle water	0.1627 cm
Material of the baffle	Stainless Steel 304
IR of barrel	187.960 cm
OR of barrel	193.675 cm
Material of the barrel	Stainless Steel 304
IR of neutron shield	194.840 cm
OR of neutron shield	201.630 cm
Material of the neutron shield	Stainless Steel 304
Width of neutron shield	32° at the 45° marks
IR of the pressure vessel liner	219.150 cm
OR of pressure vessel liner	219.710 cm
Material of the pressure vessel liner	Stainless Steel 304
IR of the pressure vessel	219.710 cm
OR of the pressure vessel	241.300 cm
Material of the pressure vessel	Carbon Steel 508

2.2 Configuration of Fuel Assemblies

The core geometry parameters are outlined over three tiers of expanding scope, describing each hierarchical component of the model shown in Figure 1. The radial core geometry is initially described, followed by a section that delineates the axial parameters. The subsequent section elaborates on the radial specifications of the grid spacers and the fuel assembly design, encompassing potential configurations of the burnable absorbers (shown in Figure 2). The comprehensive core geometry is delineated, encompassing the locations of fuel assembly enrichment, the placement of burnable absorbers, instrument tubes, shutdown banks, and control rod banks; in addition to the baffle encircling the core barrel, fuel assemblies, the reactor pressure vessel and liner, and four neutron shield panels (Shown in Figure 3-5).

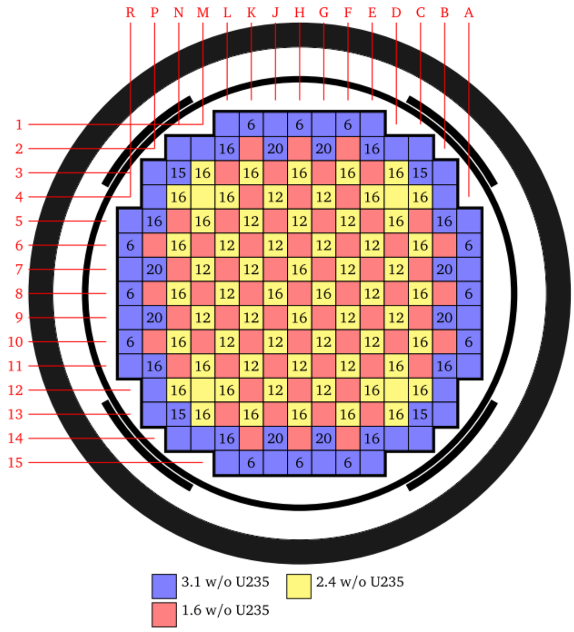

Figure 1: Fuel assembly configuration in cycle 1 (Horelik et al., 2013)

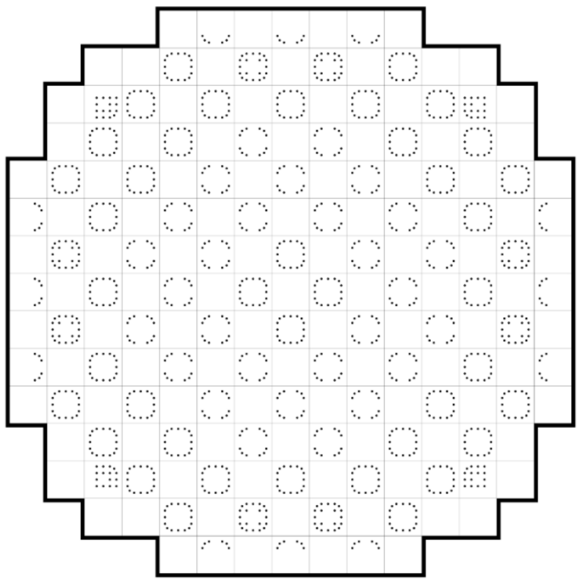

Figure 2: Detailed scale view in cycle 1 of burnable absorber pins (Horelik et al., 2013)

2.3 Monte Carlo Method in Neutronics

The answer to a problem involving the probability of an event or the mathematical expectation of a random variable can be derived from numerical experiments that yield the event's occurrence frequency, or the arithmetic mean of specific observations of the random variable. Consequently, the issue is resolved. Monte Carlo methods offer several advantages, including accurate representations of objects with stochastic properties, the capacity to model physical experiments, minimal restrictions on geometric constraints, and compatibility with parallel computing.

2.4 Simulation Approach

OpenMC uses Monte Carlo simulation to monitor a single particle at a time, with just one particle tracked per program instance. The procedure commences with problem initialization, input file analysis, data structure construction, and pseudorandom number generator initialization. The problem is further analysed for multi-group cross-section or continuous-energy data, using specialist energy-grid methodologies such as lethargy bins or union energy grids.

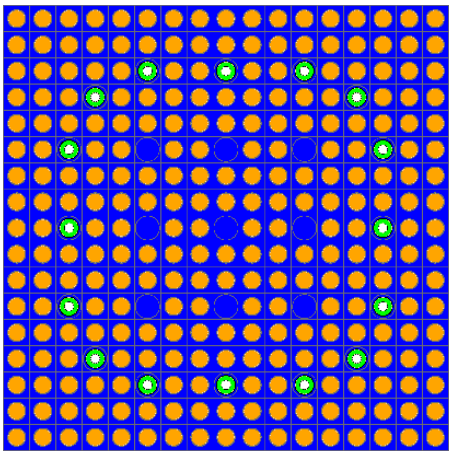

Figure 3: Typical PWR Assembly radial view

As depicted in Figure 6, the simulation is executed in a Python-based interface. After importing the OpenMC library, materials must be defined, including their isotopic composition, temperature, and density. To build the 3D solid geometry, the surfaces (e.g., planes, spheres, cylinders), the lattice (e.g., rectangular, hexagonal), and their boundary conditions (e.g., vacuum, reflective, white) must be defined. Cells with filled materials must be placed in specific universes, then used to form a lattice following the fuel configuration in the benchmark. The analysis reads nuclear cross-section data libraries in the ACE format, such as ENDF/B (Evaluated Nuclear Data File) or JEFF (Joint Evaluated Fission and Fusion File), in continuous-energy form. The transport simulation commences by initializing the particle's properties from a previously sampled source location, identifying its current cell position (Computational Reactor Physics Group & Massachusetts Institute of Technology, 2013). The simulation uses various physics models for calculations, including neutron interactions with different materials at different temperatures. The source type and number of active batches and particles can be defined in the settings. After running the simulation, the extracted data can be read from the statepoint files. For observing the 3D model, plots can be generated at high resolution from different angles and axes. For specific data collection, tallies must be defined before running the simulation, and scores can be extracted from them for calculations. After particle simulations, concluding tasks are executed, and the sample mean and variation are computed using the sum of squares and accumulated sum for each tally. All results are recorded on disk, a source file is saved upon request, and dynamically allocated memory must be deallocated (Romano et al., 2015). The SuperMC version 3.4.0 used in this work is a demo version open to everyone from the FDS team (Wu et al., 2014). Since it is a demo version, building a model from scratch was quite challenging. Hence, in this case, a pre-built 7x7 PWR-alike assembly was chosen to validate burnup calculations with both SuperMC and OpenMC. Because of the limitations of the computational tool, the simulation with only 10000 particles took more than 24 hours. About 13 steps were taken for burnup calculations; the first 5 were for 0.4 MWd/kg, and the last 8 were for 0.67 MWd/kg.

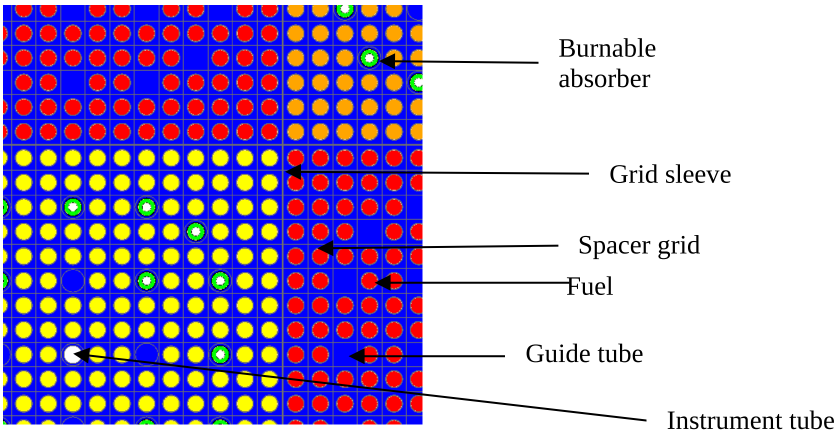

Figure 4: Grid 5 assemblies scale view with detailed spacer grid, grid sleeves, and other components

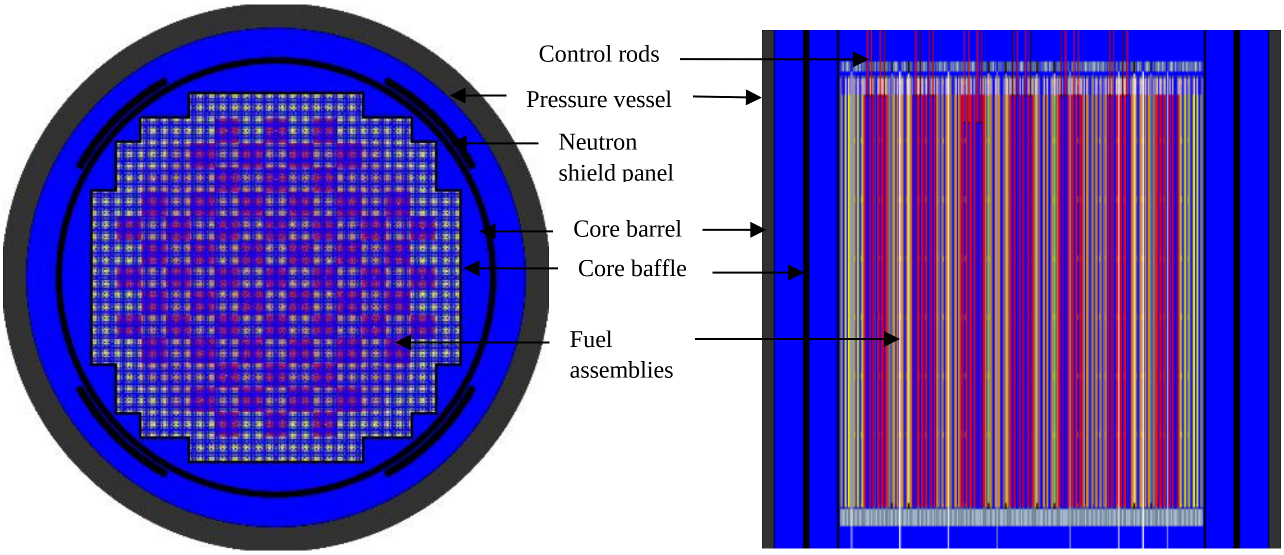

Figure 5: Radial of the PWR core (left) and axial plot of row 8 of the PWR core, where the control bank D is at bite position (right)

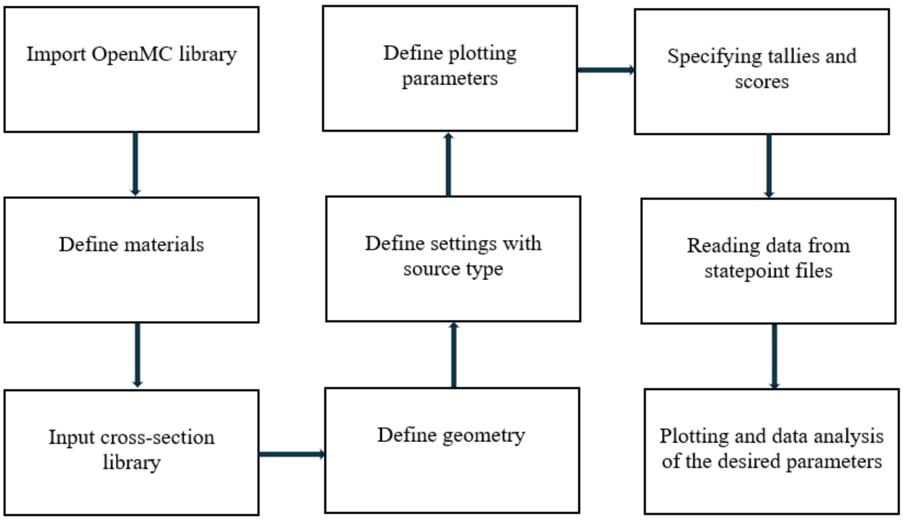

Figure 6: Simulation approach of OpenMC

3. RESULTS AND DISCUSSION

3.1 Validation of the Model

The benchmark specification provides measured data such as the critical boron concentration. In this work, the critical boron concentration has been calculated to verify the model. The other validation method was omitted for now due to limited computational resources and time constraints. The critical boron concentration is calculated using 100 batches (80 active), with 10000 particles. From Figure 7, it can be observed that, among 17 boron concentration guesses, the most frequently observed value is 975 ppm.

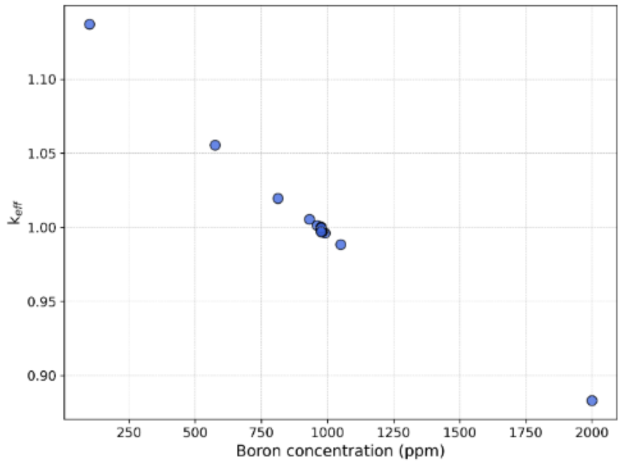

Figure 7: k_{eff} vs critical boron concentration

3.2. Effective Multiplication Factor (k_{eff}) Calculation

The core criticality calculation was conducted using 400 batches (300 inactive) with 1,000,000 particles, as shown in Table 7. The calculation was performed at the Hot Zero Power condition, with the control rod bank D at 213 steps withdrawn. It is observed that various structural components of a nuclear reactor do affect criticality, whether or not they contribute to the fission process. Here, the variation in the multiplication factor is shown in Table 8. JEFF-3.3 nuclear cross-section data library considers a higher fission probability and less absorption by U-238. The thermalization behavior in ENDF/B-VIII.0 tends to be conservative, resulting in lower fission probability. The difference between the k_{eff} values using different data libraries was calculated using the following equation:

$$\Delta k = k_{eff}(\text{JEFF-3.3}) - k_{eff}(\text{ENDF/B-VIII.0}) \qquad (1)$$

Multiplying this equation by 10^5 converts the unit to pcm. The overall differences in k_{eff} values range from 270 to 288 pcm between JEFF-3.3 and ENDF/B-VIII.0, highlighting a systemic bias between the nuclear data libraries. The material used for baffles is Stainless Steel-304, which has properties such as heat resistance and a high atomic number, indicating a high neutron reflectivity. Around 7 types of configurations of burnable absorbers are present across the core. These burnable absorbers are placed according to the neutron economy present in the different regions of the geometry. Most of the burnable absorbers are present in the assemblies with 2.4% enriched fuel, resulting in a uniform heat distribution. 8 grid spacers bound the fuel pins and the grid sleeves of the assemblies. The material in the top and bottom grid sleeves is Stainless Steel-304, and the material in the grid spacer is Inconel-718. The intermediate grid sleeve and grid spacer are made of the same material, Zircaloy. Though the presence of grid materials in the geometry is very minor compared to other structural materials (as shown in Figure-6), it is also considered for the accuracy of neutronic calculations. 5 types of control rod banks with a step width of 1.58193 cm control the reactivity following step 228 (fully withdrawn) to step 0 (fully inserted). In the Hot Zero Power condition, only bank D is partially inserted, while the other banks are fully withdrawn. Only with the insertion of control rod bank D, the deviation from the HZP condition is 761 pcm. The purpose of the boron absorbers and control rods is to control reactivity during reactor operation. With all rods out of position, the criticality seems slightly increasing from the D bank rod in bite position (213 steps withdrawn), which is about -30 pcm, indicating the insertion of negative reactivity through the control rods, as they contain boron carbide with good neutron-absorption properties and thermal stability.

3.3 Shannon Entropy

The importance of Shannon entropy in this simulation-based approach is to ensure that the data are reliable enough to be used alongside real-life scenarios and are not biased by an unconverged source distribution. The Shannon entropy in Figure 8 exhibits the convergence of the source distribution when measuring the k_{eff} value for the BEAVRS PWR reactor core. The curve shows a sharp decline in the first 100 batches, as these are initial starting guesses from random number generators. Afterwards, the value of k_{eff} converges to its final value as the source becomes more uniformly distributed within the defined area. To effectively measure Shannon entropy, the lower-left and upper-right values of the entropy mesh were set to match the uniform source distribution.

Table 7: k_{eff} values of the core at Hot Zero Power condition

BEAVRS	OpenMC	Standard Deviation	Nuclear Data Library
1.00000	1.00164	+/- 0.00008	ENDF-VIII.0

Table 8: k_{eff} values of the core with geometrical changes

Core	Nuclear Data Library	k_{eff}	Standard Deviation	Δk (pcm)	Deviation from HZP condition (pcm)
Bank D in	ENDF/B-VIII.0	0.99403	+/- 0.00009	270	761
	JEFF-3.3	0.99673	+/- 0.00009		
All control rod out	ENDF/B-VIII.0	1.00194	+/- 0.00009	278	-30
	JEFF-3.3	1.00472	+/- 0.00009		
Without Neutron Shield Panel	ENDF/B-VIII.0	1.00184	+/- 0.00008	288	-20
	JEFF-3.3	1.00472	+/- 0.00009		
Without Core Barrel	ENDF/B-VIII.0	1.00187	+/- 0.00009	283	-23
	JEFF-3.3	1.00470	+/- 0.00008		

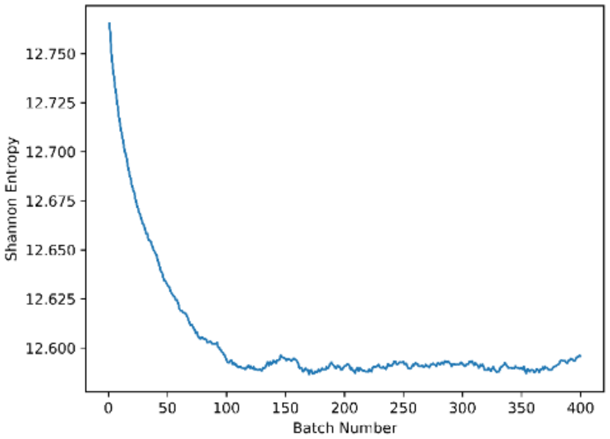

Figure 8: Convergence of Shannon entropy throughout the batches

3.4 Effective Multiplication Factor Changes with Temperature and Enrichment

Now, Figure 9 confirms the Doppler effect in a nuclear reactor. According to the Doppler effect, the reactivity, which is proportional to keff, must decrease with an increase in fuel temperature. Here, it can be observed that the BEAVRS PWR reactor core has a keff greater than 1 before 600 K. The value is gradually declining as the fuel rod temperature increases. From this curve, it can be seen that the optimal temperature for reactor operation is just below 600K. Any temperature above this will trigger an automatic shutdown system designed for the PWR reactor core. This effect is usually treated as a passive safety feature of the PWR reactor core.

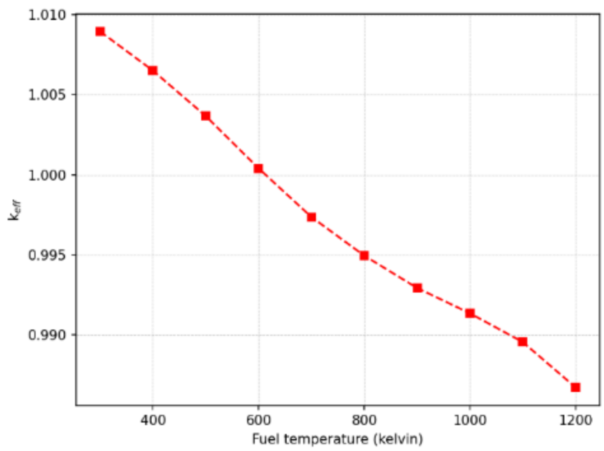

Figure 9: Confirmation of the Doppler effect by using k_{eff} vs fuel temperature in Kelvin graph

Figure 10 depicts the relationship between criticality and fuel enrichment. As there are three enrichment types in the BEAVRS PWR reactor core, the analysis was performed by changing the enrichment of one fuel type at a time. Fuel 1 does not contain any burnable absorbers, whereas Fuel 2 and 3 have a variety of burnable absorbers. For each fuel type, k_{eff} increases with increasing enrichment. However, there are slight variations in the trend. In the case of Fuel 1 with 1.6% enrichment, the value of k_{eff} is lower than in the cases of Fuel 2 with 2.4% enrichment and Fuel 3 with 3.1% enrichment. This happens because Fuel 2 and Fuel 3 have burnable absorbers, which lower k_{eff}. However, as enrichment increases, keff for fuel 1 increases rapidly, exceeding those of fuels 2 and 3. Because fuel 1 has no burnable absorbers, an increase in enrichment results in a larger increase in k_{eff}. For fuel 2, k_{eff} increases more slowly than for fuel 1, as it contains two variations of burnable absorbers (12 and 16). Fuel 3 has the slowest increase among all fuels, although it starts with a higher keff value than the others.

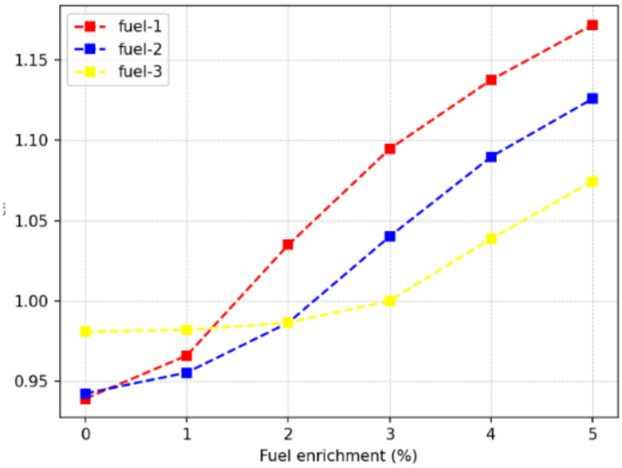

Figure 10: k_{eff} change for an increment in three types of fuel enrichment

3.5 Flux per Lethargy

For 500 energy groups from 0.1 MeV to 20 MeV, Figure 11 shows the flux per lethargy, depicting the thermal (E<0.625 eV), epithermal (0.625<E<10 eV), and fast (E>10 eV) neutron regions.

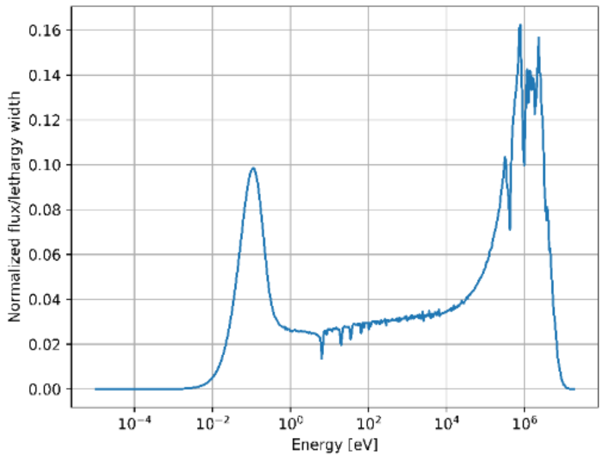

Figure 11: Normalized flux per lethargy vs energy graph for BEAVRS PWR reactor

The curve matches the typical trend for general PWR reactors. The initial peak between 10^-2 and 100 indicates the thermal-neutron flux region. The final peak at the end of the curve shows a fast-neutron flux region that is higher than the thermal-neutron flux region. This is because a fission reaction produces high-energy neutrons, which thermalize by colliding with the reactor's moderator. In the middle of these, both regions are known as the resonance region. Here, the neutrons might be captured by uranium-238 or further thermalized until they reach thermal energies.

3.6 Normalized pin-by-pin Thermal Flux Distribution

The pin-by-pin flux distribution in Figure 12 has been normalized from the unit of particle-cm per source particle to the more convenient unit of neutrons per cm^2 per second. The flux distribution visualization shows greater neutron production in assemblies without burnable absorbers, especially in those with 1.6% and 2.4% uranium-235 enrichment. The burnable absorbers in other assemblies absorb most of the neutrons, reducing the neutron flux. However, not all assemblies with 2.6% enrichment in uranium-235 exhibit high neutron flux, as they contain burnable absorbers. It also confirms that the burnable absorbers are essential for controlling overall neutron flux in the BEAVRS PWR reactor core. They help maintain a neutron economy enough to keep the reactor core critical but not supercritical. As there is a high neutron flux present near the corners of the core, neutron shield panels are placed near those corners to save leakage of neutrons through the core barrel. Another noticeable feature of the flux distribution is that it prevents the reactor core from overheating at its center. This has been achieved by placing highly enriched fuels at the outer periphery rather than at the center. Moreover, using three different types of fuel enrichment helped achieve a more uniform neutron flux.

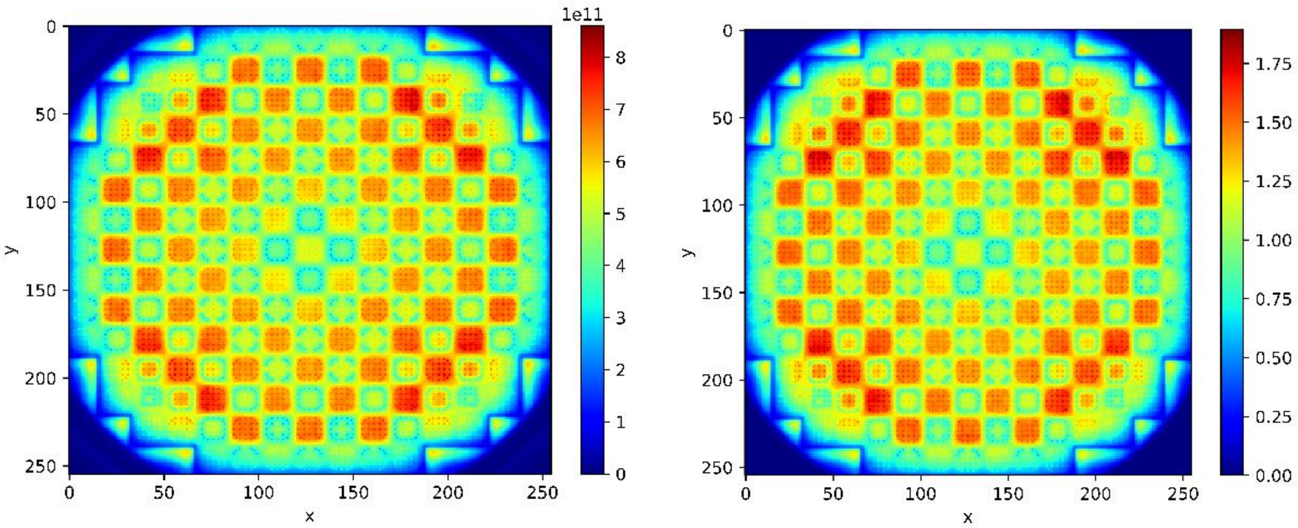

Figure 12: Normalized pin-by-pin thermal neutron flux distribution in neutrons/cm^2-sec (left) and relative thermal neutron flux across the reactor core (right)

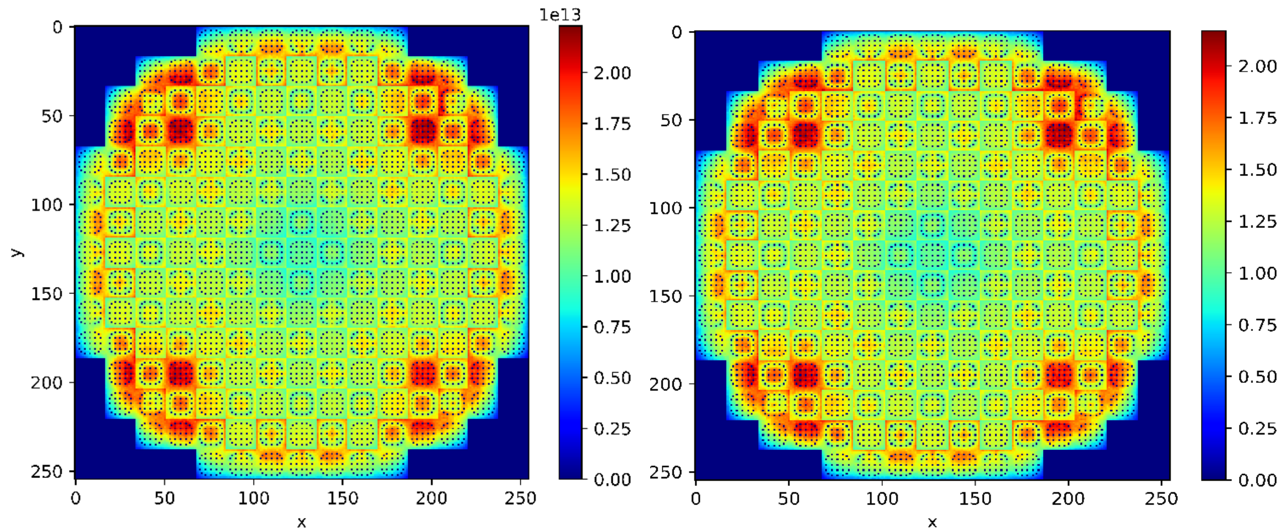

Figure 13: Normalized pin-by-pin fission rate distribution in reactions/sec (left) and relative fission rate across the reactor core (right)

3.7 Normalized Pin-by-Pin Fission Rate Distribution

Two normalization methods are used for the fission rate, as shown in Figure 13. In the first case, the fission rate was normalized by dividing the value of all pincell's fission rate by the average fission rate of all pincells of the core. Here, the relative fission rates are unitless because dividing by the same unit cancels out the units. In both cases, energy was considered a continuous source. Now, the colormap shows hot spots in the BEAVRS PWR reactor core where the power density will be higher as the fission rate is directly proportional to power. These hot spots indicate the requirement for enhanced cooling.

3.8 SuperMC Validation Using OpenMC

One objective of this work was to validate the SuperMC demo version using the OpenMC code. To do so, burnup analyses of a PWR 7x7 assembly were performed in both SuperMC and OpenMC. From the results in Figures 14 and 15, it can be observed that for 2000 and 10000 particles, both Monte Carlo codes produce curves of similar shape.

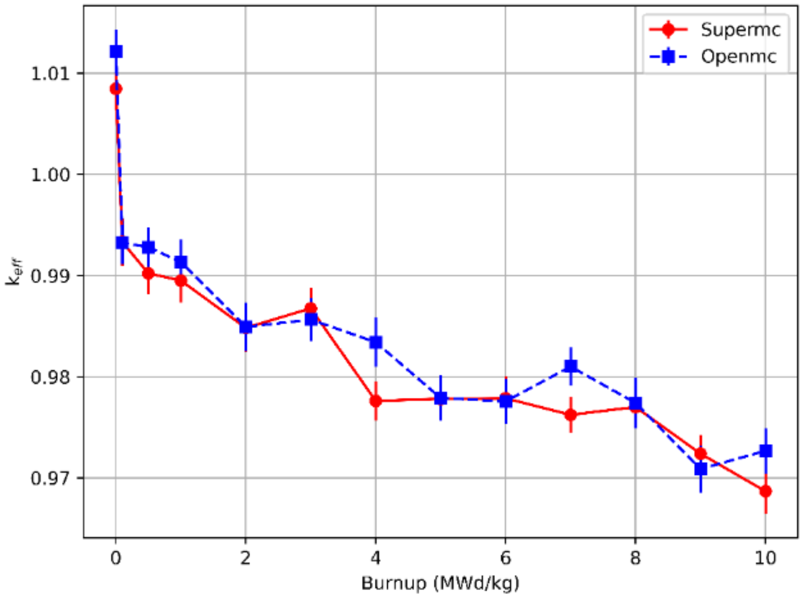

Figure 14: k_{eff} vs burnup using OpenMC and SuperMC (with 2000 particles)

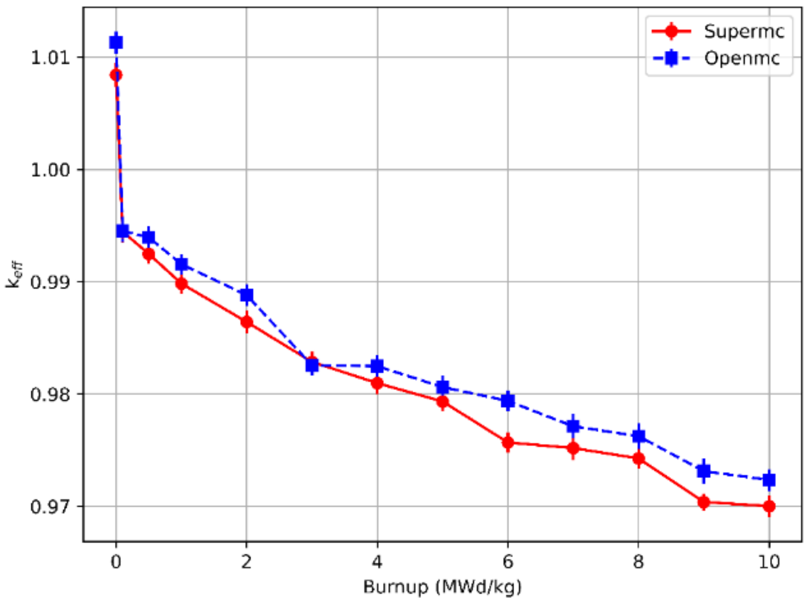

Figure 15: k_{eff} vs burnup using OpenMC and SuperMC (with 10000 particles)

At lower particle counts, both Monte Carlo codes exhibit fluctuations in k_{eff} values. It can be seen that the values sometimes rise, which is not relevant in real-life scenarios. This is because the Monte Carlo method relies primarily on a large population, which makes it easier to converge on the actual results. Low particle runs make it difficult for k_{eff} to converge to the actual result. For this reason, higher particles are taken into account for the calculation of any sort. In this case, both Monte Carlo codes show a similar trend of decrease in k_{eff} values. For 2000 particles, there are many aberrations for OpenMC and SuperMC. However, for 10000 particles, both start to show similar decreases. The sharp drop at the beginning shows the initial guess, which is essential for convergence.

4. CONCLUSIONS

This research primarily focuses on determining the neutronic parameters of the BEAVRS PWR, with the ultimate goal of validating the SuperMC demo code using OpenMC. The validation has been achieved by using the same geometry and material composition in both OpenMC and SuperMC. The results are accurate enough for the limited computational power available. The JEFF-3.3 nuclear cross-section library generates slightly higher effective multiplication factors for different conditions than ENDF/B-VIII.0, with a standard deviation around +/- 0.00008. It is also observed that hotspots typically occur around assemblies with no burnable absorbers and higher-enriched fuel. To prevent leakage from these hotspots, the neutron shield panels are placed outside the core barrel accordingly. High-resolution pin-by-pin thermal neutron flux and fission rate map confirmed that the BEAVRS core design effectively flattens the power distribution, with peak thermal flux reaching approximately 8×10^{11} neutrons/cm^2-sec, considering pin-by-pin calculation. Higher accuracy in overall analyses could be achieved using higher computational power. The OpenMC and SuperMC approaches developed for the PWR-based BEAVRS benchmark can be adapted for the analysis of the PWR-type VVER-1200 reactor at the Rooppur Nuclear Power Plant, which is expected to commence operation in the 2026–2027 timeframe.

ACKNOWLEDGMENTS

The authors would like to express their gratitude to the Department of Nuclear Science and Engineering, MIST, for their support during the simulation, and to the FDS team for providing the SuperMC demo version.

DATA AVAILABILITY STATEMENT

Datasets generated during the current study are available from the corresponding author upon reasonable request.

FUNDING DECLARATION

This research was self-funded.

ETHICS APPROVAL

This study is an engineering experimental investigation. The MIJST Research Ethics Committee has confirmed that formal ethical approval was not required.

ETHICS, CONSENT TO PARTICIPATE, AND CONSENT TO PUBLISH

Not applicable.

COMPETING INTERESTS

The authors declare that they have no competing interests.

AUTHOR CONTRIBUTIONS

Author 1: Data collection, Methodology, Data Curation, Formal Analysis, Writing - Original Draft & formatting.
Author 2: Methodology, Data Curation, Formal Analysis, Writing - Draft Review & Editing.
Author 3: Supervision, Conceptualization, Writing - Draft Review.

ARTIFICIAL INTELLIGENCE ASSISTANCE STATEMENT

Portions of this manuscript were assisted by an artificial intelligence language model (ChatGPT, OpenAI). The tool was used solely for language editing, text refinement, and improving clarity. All content, data interpretation, analysis, conclusions, and final decisions were produced, verified, and approved by the authors. The authors take full responsibility for the accuracy and integrity of the manuscript.

CONFLICT OF INTEREST DECLARATION

The authors declare that they have no conflicts of interest.

REFERENCES

Alamri, K. A., Alqahtani, M. M., Alomari, A. S., & Almarshad, A. I. (2024). Neutronic Analysis of Accident-Tolerant cladding materials in 3D Full core BEAVRS PWR Benchmark using OpenMC Code. *International Journal of Energy Research*, *2024*, 1–22. https://doi.org/10.1155/2024/8811265

Albugami, A. O., Alomari, A. S., & Almarshad, A. I. (2023). Modeling and simulation of VERA core physics benchmark using OpenMC code. *Nuclear Engineering and Technology*, *55*(9), 3388–3400.

Bahadir, T. (2021). BEAVRS BENCHMARK EVALUATION WITH CASMO5 AND SIMULATE5. *EPJ Web of Conferences*, *247*, 06022. https://doi.org/10.1051/epjconf/202124706022

Collins, B., Godfrey, A., Stimpson, S., & Palmtag, S. (2020). Simulation of the BEAVRS benchmark using VERA. *Annals of Nuclear Energy*, *145*, 107602. https://doi.org/10.1016/j.anucene.2020.107602

Coloma, W. A., De Lima Reis, N. P. A., Da Silva, N. C. a. M., & Lima, N. C. P. B. (2022). Macroscopic cross section generation with WIMS-ANL for a PWR. *Brazilian Journal of Radiation Sciences*, *10*(3A). https://doi.org/10.15392/2319-0612.2022.1948

Computational Reactor Physics Group & Massachusetts Institute of Technology. (2013). *The OpenMC Monte Carlo Code — OpenMC documentation*. (Extracted on

March. 4, 2026). Source: https://docs.openmc.org/

Darnowski, P., & Pawluczyk, M. (2019). Analysis of the BEAVRS PWR benchmark using SCALE and PARCS. *Nukleonika*, *64*(3), 87–96. https://doi.org/10.2478/nuka-2019-0011

Darnowski, P., & Pawluczyk, M. (2022). Simulations of the BEAVRS PWR with SCALE and PARCS. In *International Agreement Report* (NUREG/IA-0529). U.S. Nuclear Regulatory Commission. https://www.researchgate.net/publication/366407772_Simulations_of_the_BEAVRS_PWR_with_SCALE_and_PARCS

Fröhlicher, K., Salino, V., & Hébert, A. (2021). Investigating fission distribution behavior under various homogenization techniques for asymmetrical fuel assemblies and different reflector equivalence methods. *Annals of Nuclear Energy*, *157*, 108221. https://doi.org/10.1016/j.anucene.2021.108221

Gunow, G., Forget, B., & Smith, K. (2019). Full core 3D simulation of the BEAVRS benchmark with OpenMOC. *Annals of Nuclear Energy*, *134*, 299–304. https://doi.org/10.1016/j.anucene.2019.05.050

Hassan, M. (2020). Simulation of a full PWR core with MCNP6. *International Journal of Science and Research (IJSR)*, *9(9)*, 913–918. https://doi.org/10.21275/SR20916224433

Hassan, M., & Hassan, M. (2021). Simulation of BEAVRS benchmark at Hot Zero Power using MCNP6. *Arab Journal of Nuclear Sciences and Applications*, *54*(2), 73–81. https://doi.org/10.21608/ajnsa.2021.33692.1371

Horelik, N., Herman, B., Forget, B., & Smith, K. (2013). Benchmark for Evaluation and Validation of Reactor Simulations (BEAVRS), v1.0.1. In Proceedings of the *International Conference on Mathematics and Computational Methods Applied to Nuclear Science and Engineering*
https://doi.org/10.1016/j.anucene.2017.09.045
https://doi.org/10.1016/j.net.2019.09.007
https://doi.org/10.1016/j.net.2020.02.015
https://doi.org/10.1016/j.net.2023.05.036

Jeon, S., & Kochunas, B. (2024). Verification and Validation of the VANGARD Pinwise Nodal Code with Analyses of BEAVRS. *Nuclear Science and Engineering*, 1–24. https://doi.org/10.1080/00295639.2024.2421095

Kim, K. M., Im, J., Choi, N., Lee, H. G., & Joo, H. G. (2023). High-Performance and High-Fidelity GPU-Based Monte Carlo solutions to the BEAVRS benchmark. *Nuclear Science and Engineering*, *197*(8), 1823–1844. https://doi.org/10.1080/00295639.2022.2148812

Kim, K., Jeon, B., Ward, A., Mertyurek, U., Jessee, M., & Wieselquist, W. (2024). Validation of the SCALE/Polaris−PARCS Code Procedure with the ENDF/B-VII.1 AMPX 56-Group Library: Pressurized Water Reactor. *Journal of Nuclear Engineering*, *5*(3), 246–259. https://doi.org/10.3390/jne5030017

Leppänen, J., & Mattila, R. (2016). Validation of the Serpent-ARES code sequence using the MIT BEAVRS benchmark – HFP conditions and fuel cycle 1 simulations. *Annals of Nuclear Energy*, *96*, 324–331. https://doi.org/10.1016/j.anucene.2016.06.014

Leppänen, J., Mattila, R., & Pusa, M. (2014). Validation of the Serpent-ARES code sequence using the MIT BEAVRS benchmark – Initial core at HZP conditions. *Annals of Nuclear Energy*, *69*, 212–225. https://doi.org/10.1016/j.anucene.2014.02.014

Li, Y., Zhang, B., He, Q., Wang, D., Wu, H., Cao, L., & Shen, W. (2018). Development and verification of PWR-core fuel management calculation code system NECP-Bamboo: Part I Bamboo-Lattice. *Nuclear Engineering and Design*, *335*, 432–440. https://doi.org/10.1016/j.nucengdes.2018.05.030

Liu, S., Liang, J., Wu, Q., Guo, J., Huang, S., Tang, X., Li, Z., & Wang, K. (2016). BEAVRS full core burnup calculation in hot full power condition by RMC code. *Annals of Nuclear Energy*, *101*, 434–446. https://doi.org/10.1016/j.anucene.2016.11.033

Oh, T., Jeong, Y., Khalefih, H., & Kim, Y. (2023). Development and validation of multiphysics PWR core simulator KANT. *Nuclear Engineering and Technology*, *55*(6), 2230–2245. https://doi.org/10.1016/j.net.2023.02.025

Palmi, K., Kubinski, W., & Darnowski, P. (2024). Prediction of the evolution of the nuclear reactor core parameters using artificial neural network. *Annals of Nuclear Energy*, *211*, 110891. https://doi.org/10.1016/j.anucene.2024.110891

Park, H. J., & Cho, J. Y. (2023). Establishment of DeCART/MIG stochastic sampling code system and Application to UAM and BEAVRS benchmarks. *Nuclear Engineering and Technology*, *55*(4), 1563–1570. https://doi.org/10.1016/j.net.2023.02.027

Park, H. J., Kim, S. J., Kwon, H., & Cho, J. Y. (2020). BEAVRS benchmark analyses by DeCART stand-alone calculations and comparison with DeCART/MATRA multi-physics coupling calculations. *Nuclear Engineering and Technology*, *52*(9), 1896–1906.

Pediz, G., Yılmazer, A., & Tombakoğlu, M. (2023). Transport equivalent full core neutronics calculations via the finite volume method and optimized diffusion parameters. *Progress in Nuclear Energy*, *165*, 104935. https://doi.org/10.1016/j.pnucene.2023.104935

Ren, C., He, L., Lei, J., Liu, J., Huang, G., Gao, K., Qu, H., Zhang, Y., Li, W., Yang, X., & Yu, T. (2023). Neutron transport calculation for the BEAVRS core based on the LSTM neural network. *Scientific Reports*, *13*(1), 14670. https://doi.org/10.1038/s41598-023-41543-1

Romano, P. K., Horelik, N. E., Herman, B. R., Nelson, A. G., Forget, B., & Smith, K. (2015). OpenMC: A state-of-the-art Monte Carlo code for research and development. *Annals of Nuclear Energy*, *82*, 90–97. https://doi.org/10.1016/j.anucene.2014.07.048

Ryu, M., Jung, Y. S., Cho, H. H., & Joo, H. G. (2015). Solution of the BEAVRS benchmark using the nTRACER direct whole core calculation code. *Journal of Nuclear Science and Technology*, *52*(7–8), 961–969. https://doi.org/10.1080/00223131.2015.1038664

Suzuki, M., & Nagaya, Y. (2023). Whole core analysis of BEAVRS benchmark for hot zero power condition using MVP3 with JENDL-5. *Journal of Nuclear Science and Technology*, *61*(2), 177–191. https://doi.org/10.1080/00223131.2023.2279299

Tatsuya, F., & Tomohiro, S. (2021). ANALYSIS OF THE BEAVRS BENCHMARK USING CASMO5/SIMULATE5 WITH JENDL-4.0 AND ENDF/B-VII.1. *EPJ Web of Conferences*, *247*, 02014. https://doi.org/10.1051/epjconf/202124702014

Tuominen, R., & Valtavirta, V. (2022). BEAVRS pin-by-pin calculations with Ants-SUBCHANFLOW-SuperFINIX code system. *Annals of Nuclear Energy*, *180*, 109447. https://doi.org/10.1016/j.anucene.2022.109447

Valtavirta, V., Rintala, A., & Lauranto, U. (2022). Validating the serpent-ants Calculation Chain Using BEAVRS Fresh Core Hot Zero Power Data. *Journal of Nuclear Engineering and Radiation Science*, *8*(4). https://doi.org/10.1115/1.4052731

Wang, K., Liu, S., Li, Z., Wang, G., Liang, J., Yang, F., Chen, Z., Guo, X., Qiu, Y., Wu, Q., Guo, J., & Tang, X. (2017). Analysis of BEAVRS two-cycle benchmark using RMC based on the full core detailed model. *Progress in Nuclear Energy*, *98*, 301–312. https://doi.org/10.1016/j.pnucene.2017.04.009

Wang, Z., Wu, B., Hao, L., Liu, H., & Song, J. (2017). Validation of SuperMC with BEAVRS benchmark at Hot Zero Power condition. *Annals of Nuclear Energy*, *111*, 709–714.

Wu, Y., Song, J., Zheng, H., Sun, G., Hao, L., Long, P., & Hu, L. (2014). CAD-based Monte Carlo program for integrated simulation of nuclear system SuperMC. *Annals of Nuclear Energy*, *82*, 161–168. https://doi.org/10.1016/j.anucene.2014.08.058

Yang, J., Wu, H., Guo, L., Li, Y., Li, X., Wang, S., Hao, T., & Ji, W. (2021). Validation of NECP-Bamboo with BEAVRS and AP1000 measurements. *Nuclear Engineering and Design*, *376*, 111110. https://doi.org/10.1016/j.nucengdes.2021.111110

Yu, J., Lee, H., Kim, H., Zhang, P., & Lee, D. (2019). Simulations of BEAVRS benchmark cycle 2 depletion with MCS/CTF coupling system. *Nuclear Engineering and Technology*, *52*(4), 661–673.

Yu, J., Lee, H., Lemaire, M., Kim, H., Zhang, P., & Lee, D. (2019a). MCS based neutronics/thermal-hydraulics/fuel-performance coupling with CTF and FRAPCON. *Computer Physics Communications*, *238*, 1–18. https://doi.org/10.1016/j.cpc.2019.01.001

Yu, J., Lee, H., Lemaire, M., Kim, H., Zhang, P., & Lee, D. (2019b). Fuel performance analysis of BEAVRS benchmark Cycle 1 depletion with MCS/FRAPCON coupled system. *Annals of Nuclear Energy*, *138*, 107192. https://doi.org/10.1016/j.anucene.2019.107192

Zhang, B., Liu, Z., Yuan, X., Zhang, Y., Zhou, J., Tang, H., & Xiao, Y. (2024). Validation of DDC-3D code system for neutronics and thermal-hydraulics coupling analysis using BEAVRS benchmark. *Nuclear Engineering and Design*, *429*, 113583. https://doi.org/10.1016/j.nucengdes.2024.113